Internal Resonance and Stall Flutter Interactions in a Pitch-Flap Wing in the Wind-Tunnel

E. Verstraelen, G. Kerschen, G. Dimitriadis

Department of Aerospace and Mechanical Engineering, University of Liège, Belgium

Abstract

Nonlinear aeroelastic phenomena such as store-induced LCOs, transonic buzz and stall flutter are the burden or modern aircraft: they reduce the performance and can even limit the flight envelope in both civil and military cases. Several nonlinear setups were studied experimentally in the last decades by the scientific community but most of them have pitch and plunge degrees of freedom and feature a rigid wing. In this paper, we study a new nonlinear aeroelastic apparatus that features nonlinear pitch and flap degrees of freedom, coupled with a flexible wing. The model is tested experimentally in the wind tunnel to determine its dynamic behaviour. Preliminary observations demonstrate that the system undergoes a supercritical Hopf bifurcation due to the hardening nonlinearity followed by an amplitude jump that is the consequence of either dynamic stall (i.e. stall flutter) or internal resonance (i.e. interaction between the hardening nonlinearity and higher modes).

Keywords: Wind-Tunnel Testing, Nonlinear Aeroelasticity, Stall Flutter, Internal Resonance, Bifurcations.

1 INTRODUCTION

Aeroelasticity is the result of mutual interactions between vibrating modes of a flexible structure and aerodynamic loads. It can lead to linear flutter or, in the nonlinear case, to limit cycle oscillations (LCOs) such as store-induced LCOs, transonic buzz and stall flutter. Such phenomena limit the performance or even the flight envelope of aircraft and have therefore been widely studied by the scientific community during the last 30 years.

A wide range of experimental setups was developed in order to make and validate models or simply to understand the underlying physics of different aeroelastic phenomena. Most of them are characterised by a stiff wing with pitch and plunge degrees of freedom (DOFs) and sometimes a control surface DOF. Setups with a linear structural part and aerodynamic nonlinearity were developed by Amandolese et al.[1] , Abdul Razak et al.[2][3] and Dimitriadis et al.[4] to study stall flutter. Poirel et al.[5] studied laminar separation flutter thanks to another linear setup. The Pitch And Plunge Apparatus (PAPA) was used to test flutter control mechanisms at transsonic airspeeds by Mukhopadhvay V.[6]. Several structurally nonlinear setups were built such as the Nonlinear Aeroelastic Testbed Apparatus (NATA) (O'Neil et al.[7] and Silva et al.[8]) which uses a cam system to get different continuous nonlinearities on the pitch and plunge DOFs. The NATA was also used by Dowell et al.[9] for teaching purposes. Abdelkefi et al.[10] developed and modelled a different setup using a leaf spring. Conner et al.[11] extensively studied both numerically and experimentally the effects of freeplay in control surfaces. Tang et al.[12] tested an aileron flexible in flap, lag and torsion with freeplay at the root. Most of these structurally nonlinear setups use ball bearings which also introduces nonlinear frictions and hysteresis.

The apparatus we propose in the present study is the Nonlinear Pitch and Flap Wing (NLPFW). It is a flat plate with pitch and flap DOFs inspired by the wing invented by Hancock et al.[13] and used in a book by Wright et al.[14] for teaching purposes. It is structurally hardening and does not feature any bearing thanks to specially designed leaf spring and clamps inspired by the work of Platten et al.[15]. Separation of the airflow occurs at high oscillation amplitudes, which also leads to aerodynamic nonlinearity. This paper presents the NLPFW and provides an experimental investigation of its dynamic behaviour at both wind-off and wind-on conditions. Particular emphasis is given to the appearance of stall flutter and internal resonance phenomena.

2 EXPERIMENTAL SETUP

The experimental apparatus is installed in the Wind-Tunnel of the University of Liège. The model is designed to achieve very low damping ($\approx 0.3\%$ at wind-off conditions) and flutter at an airspeed of around 12m/s. To achieve such a low structural damping, the setup does not use any bearings or rotational springs. The pitch and flap restoring torques are provided by a specially designed leaf spring and nonlinear clamps.

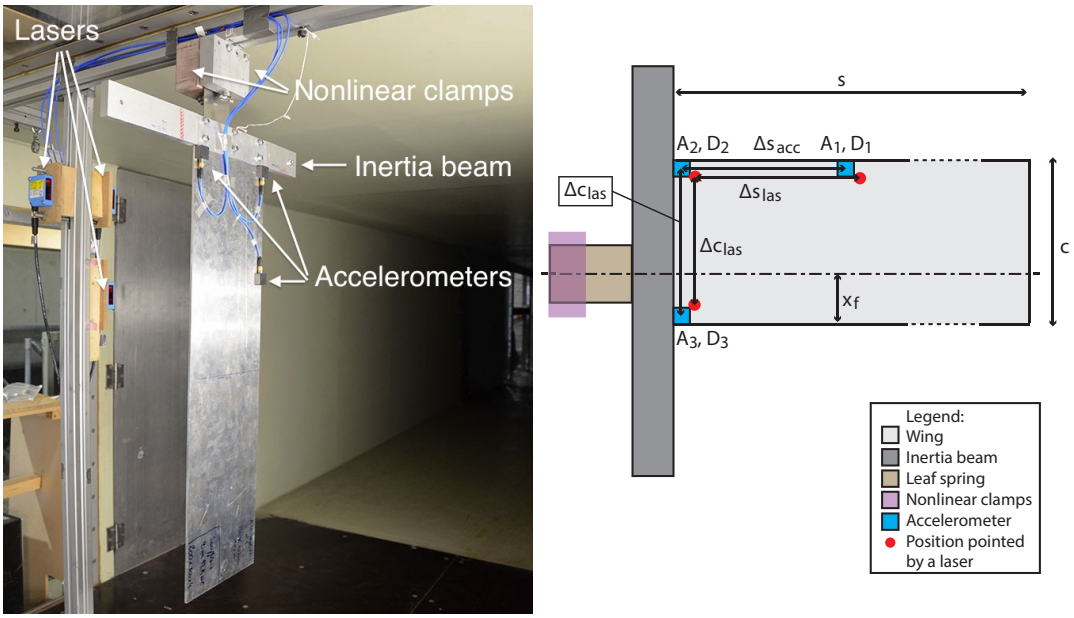

(a) Photo of the setup in the wind-tunnel

(b) Diagram showing transducer locations and major components of the NLPFW

Figure 1: Experimental setup showing wing, support and transducers

The design of the NLPFW (shown in Fig.1) is based on the Hancock wing theoretically developed by J.Hancock during the 80's [13] and drawn in Fig.2. It is a stiff thin rectangular unswept flat plate with span $s = 750$ mm, chord $c = 200$ mm, thickness $t = 4$ mm and an aspect ratio of 3.75. It is hinged at its root at $0.3c$ from the leading edge. As a result it features two rigid DOFs: a pitch rotation θ and a flap rotation γ. The axis system OXYZ is fixed. The flexural axis, e_s, is parallel to the leading edge and passes by the hinge while the axis e_c is the root of the wing. The pitch angle θ is defined as the angle formed by the axis e_c and X i.e. it measures the rotation around the axis e_s. The flap angle γ is the angle formed by the axis e_s and Z which means that it measures the rotation around the axis e_c.

The stiffness in both pitch and flap is provided by a thin C75S leaf spring. It is 100 mm long, 70 mm large and 0.7 mm thick. It is clamped on the flat plate and on the roof of the test section of the wind-tunnel using two nonlinear clamps. Fig.3(a) draws the geometry of these clamps and Fig.3(b) plots the nonlinear restoring torque of the pitch DOF and a third order fitting. It was measured statically by applying masses to the pitch DOF and measuring the resulting deflection using a digital inclinometer with a resolution of 0.1°. The flap stiffness is linear in the displacement range considered.

Finally, a 500 mm $\times$ 50 mm $\times$ 15 mm beam is bolted at the junction between the flat plate and the leaf spring (see Fig.1(a) and 1(b)). It increases the rotational inertia of the system and consequently decreases its flutter speed to make it in the target speed range: [10-15] m/s. Table 1 summarises the wind-off characteristics of the NLPF.

The displacements are measured by the means of 3 Sick OD2-P300W200I0 laser sensors with a sensitivity of 9.6 mV/mm and a range of $100 - 500$ mm. The accelerations are measured using 3 MEMS DC accelerometers with a sensitivity of 100mV/G and a

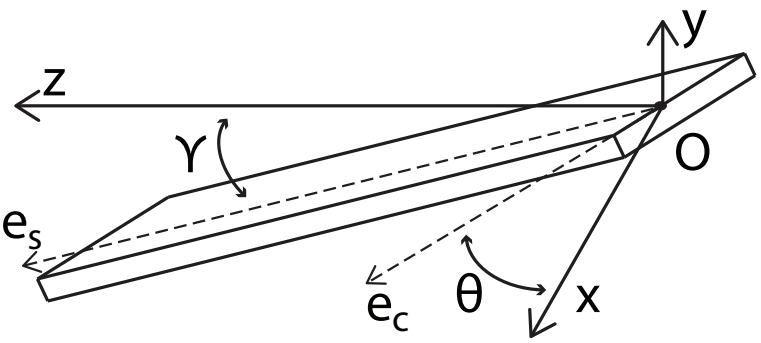

Figure 2: Schematic of the Hancock Wing

Caracteristic	Symbol	value	Unit
Dimensions of the wing:			
Span	s	750	[mm]
Chord	c	200	[mm]
Thickness	t	4	[mm]
Flap properties			
Linear stiffness	K_γ	≈ 5	[Nm/rad]
Inertia	I_γ	0.42	[kg m^2]
Damping	ζ_γ	≈ 1	[%]
Frequency	f_γ	0.85	[Hz]
Pitch properties			
Inertia	I_θ	0.029	[kg m^2]
Linear stiffness coefficient	K_θ	10.3	[Nm/rad]
Quadratic stiffness coefficient	$K_{\theta,2}$	≈ 0	[Nm/rad^2]
Cubic stiffness coefficient	$K_{\theta,3}$	858	[Nm/rad^3]
Damping	ζ_θ	≈ 0.3	[%]
Frequency	f_θ	3.1	[Hz]
Position of the sensors			
Distance between A_1 and A_2	Δs_{acc}	200	[mm]
Distance between A_2 and A_3	Δc_{acc}	180	[mm]
Distance between D_1 and D_2	Δs_{las}	205.5	[mm]
Distance between D_2 and D_3	Δc_{acc}	168.5	[mm]

Table 1: Wind-off characteristics of the NLPF

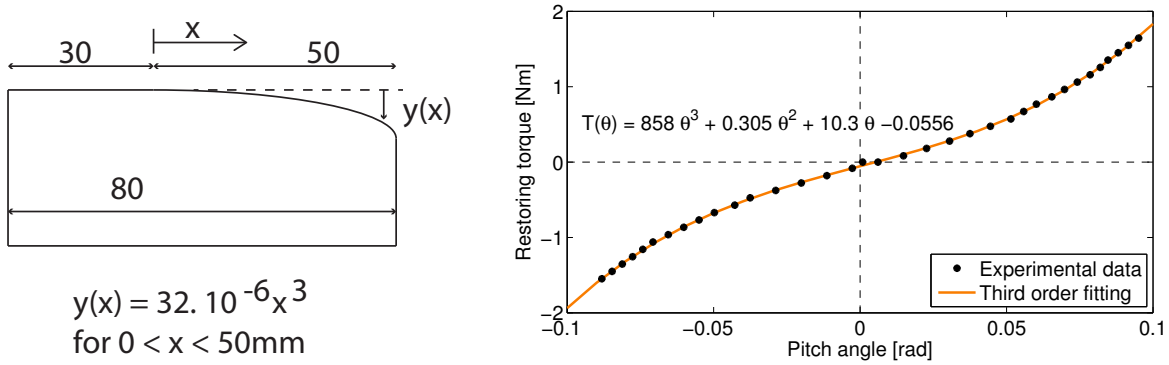

(a) Sketch of the clamps

(b) Experimental restoring torque curve of the pitch DOF

Figure 3: Characteristics of the nonlinear clamps

range of $\pm$ 30G. The sampling frequency of these two instruments is set to 1000Hz. The position of the sensors is shown in Fig.1(b). The accelerometers A_2 & A_3 and the lasers D_2 & D_3 are placed at the root of the wing. As a result there is no torsion of the flat plate and the pitch accelerations and displacements can be computed as in displayed in Eqn. 1 and 2 assuming a stiff plate.

$$\ddot{\theta} = (A_2 - A_3)(\Delta c_{acc})^{-1} \qquad [rad/s^2] \tag{1}$$

$$\theta = \arctan[(D_2 - D_3)(\Delta c_{las})^{-1}] \qquad [rad] \tag{2}$$

At low energy levels -typically before the flutter speed- this hypothesis is also valid for the flap accelerations, measured using accelerometers A_1 and A_2 (see Eqn. 3) and for the flap displacement, measured using lasers D_1 and D_2 (see Eqn. 4).

$$\ddot{\gamma} = (A_1 - A_2)(\Delta s_{las})^{-1} \qquad [rad/s^2] \tag{3}$$

$$\gamma = \arctan[(D_1 - D_2)(\Delta s_{las})^{-1}] \qquad [rad] \tag{4}$$

At high energy levels -typically the LCOs cases- the rigid plate hypothesis is not valid. A new variable ϕ (see Eqn. 5 and 6) is introduced to quantify the deformations of the flat plate: subtracting the signal of accelerometer A_2 (or laser D_2) from the signal of accelerometer A_1 (or laser D_1) cancels the pitch contribution and gives an idea of displacements and accelerations due to the vibrations of the plate.

$$\ddot{\phi} = A_1 - A_2 \qquad [m/s^2] \tag{5}$$

$$\phi = D_1 - D_2 \qquad [m] \tag{6}$$

3 RESULTS

Three types of tests were carried out to study this system:

1. Modal analysis at wind-off is performed.
2. The variation of the modal parameters with the airspeed is investigated.
3. The super-critical behaviour of the system is explored through the limit cycles (LCOs) amplitudes frequencies and mode-shapes.

3.1 Wind-off modal analysis of the system

Hammer testing was used to carry out mind-off modal analysis. The wing was impacted five times in 24 different locations using a hammer instrumented with a force gauge. The response was measured with a single accelerometer placed on the trailing edge at the tip of the wing. Since it is very difficult to excite the leaf spring with the hammer its deflections are extracted from a model with

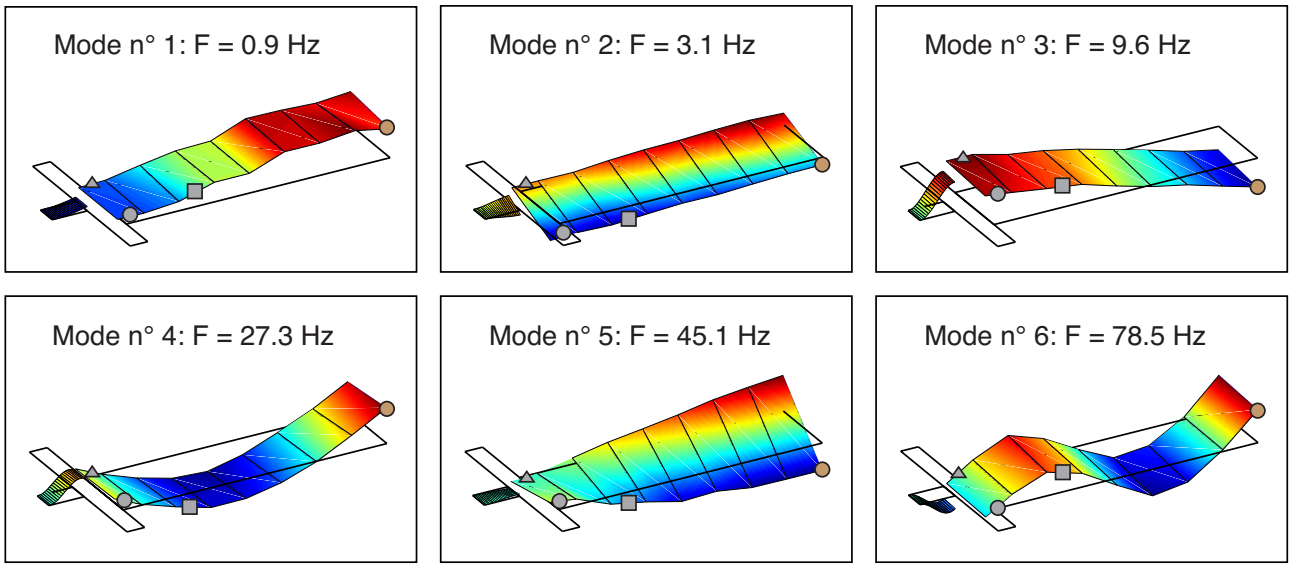

Figure 4: Modes shapes of the NLPF. The brown dots indicate the position of the accelerometer used for the modal analysis. The grey square, dots and triangles respectively show the position of the accelerometers A_1 A_2 & A_3.

shell finite elements of the whole structure computed by the means of the Finite Element package SAMCEF. Figure 4 shows the first six modes and the positions of the three accelerometers A_1 A_2 & A_3. No clear modes were identified between 10 and 27 Hz, probably due to nonlinear effects. A shaker test at different vibration levels is planned in the near future. The model predicts the existence of an in-plane mode between modes 3 and 4. Nevertheless this mode is aligned with the airflow and should not contribute greatly to the important dynamics of the system. The six mode shapes are the following:

1. First mode: first flexural mode of the leaf spring and no deformation of the flat plate. It is equivalent to γ, the flap DOF of the Hancock wing.
2. Second mode: first torsional mode of the leaf spring and no deformation of the flat plate. It is equivalent to θ, the pitch DOF of the Hancock Wing.
3. Third mode: second flexural mode of the leaf spring and first flexural mode of the flat plate.
4. Fourth mode: second flexural mode of the leaf spring and second flexural mode of the flat plate.
5. Fifth mode: first torsional mode of the flat plate.
6. Sixth mode: second flexural mode of the leaf spring and third flexural mode of the flat plate.

3.2 Wind-on study of the system

3.2.1 VARIATION OF THE MODAL PARAMETERS WITH AIRSPEED

The variation of the damping and frequency of the system were studied using free decays. For each stabilised airspeed, the system was given an initial pitch and flap angle then was released. Figure 5 shows pitch and flap responses at three different airspeeds. The damping of the pitch angle increases slowly while the damping of the flap angle becomes large. The wind-on frequency of the system was computed from these free decays using Fast Fourier Transform (FFT) or Wavelet Analysis. The damping was computed using an exponential curve fit of the Hilbert Transform of the responses. Figure 6 shows the variation of frequency and damping of the first two modes with airspeed. It is a classical frequency vs airspeed diagram of a system that flutters: the flap damping increases monotonously while the pitch damping first increases until 9m/s then decreases until flutter occurs. The modal properties of the flap mode are very scattered because the damping was so high that the system could only undergo a few oscillations before

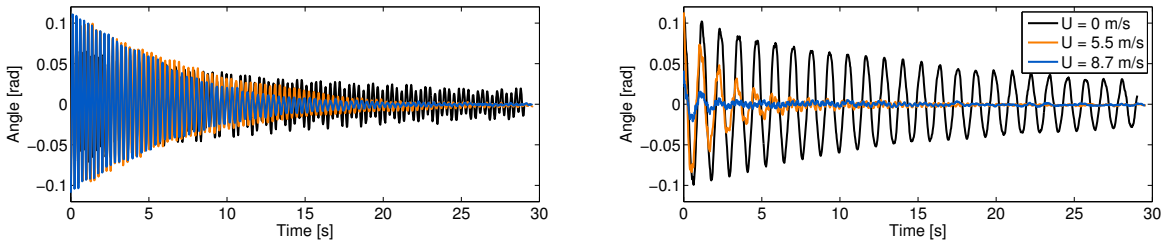

(a) Pitch response (b) Flap response

Figure 5: Response of the system at sub-critical airspeeds released from an initial pitch and flap angle of 0.1 rad

going back to rest. The frequency diagram is also quite common for flutter systems: the pitch and flap frequencies move closer to each other as the airspeed increases until flutter occurs. The variation of the frequency and the damping of modes 3 to 6 is not displayed here because these modes are not influenced in the velocity range considered, which means that the do not participate in the flutter mechanism.

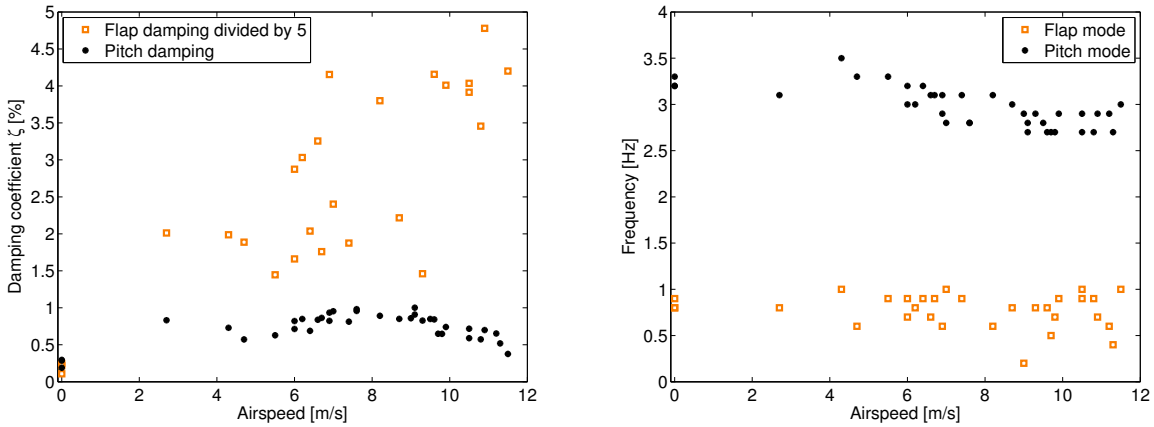

(a) Damping (b) Frequency

Figure 6: Variation of the modal parameters of the pitch and flap DOFs with the airspeed before the flutter

3.2.2 LIMIT CYCLE OSCILLATION AMPLITUDE AND SHAPE VARIATION WITH AIRSPEED

Figs.7(a) & 7(b) respectively show the evolution of the pitch Root Mean Square (RMS) acceleration and displacement (right) with airspeed. The black dots correspond to increasing airspeed tests while the orange squares are related to decreasing airspeed tests. Both sets of points appear to lie on the same curve, which suggests that there is no hysteresis in the system. The bifurcation at 11.5 m/s is a supercritical Hopf: the LCOs were self-excited and manually exciting the system using a rope did not lead to a jump on a branch of higher amplitude. The displacement curve and the acceleration curve both show similar trends: the LCOs start at 11.5 m/s and their amplitude increases smoothly up to 13.5 m/s. At 13.5 m/s a jump occurs: the RMS acceleration is increased by a factor of 5 and the RMS displacement is increased by a factor of 2. After this jump, the amplitude increases slowly with airspeed. A test with wool tufts showed that separation of the airflow occurs after the jump for pitch amplitudes of around 8°. Fig.8(b) to 8(e) contains 4 pictures of the wool tufts placed as displayed in Fig.8(a) at four time instances of the same half cycle. The top row of tufts, which corresponds to the red one in Fig.8(a), lies near the leading edge of the wing while the bottom row, which corresponds

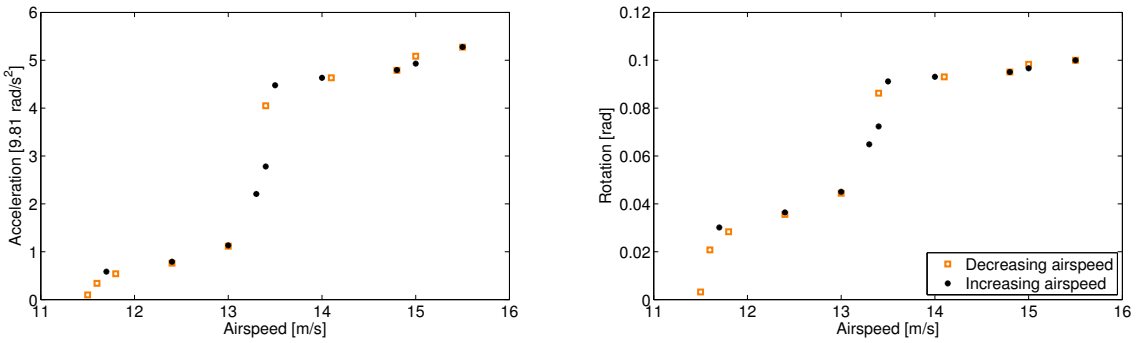

(a) RMS acceleration (b) RMS displacement

Figure 7: Bifurcation diagram of the pitch DOF

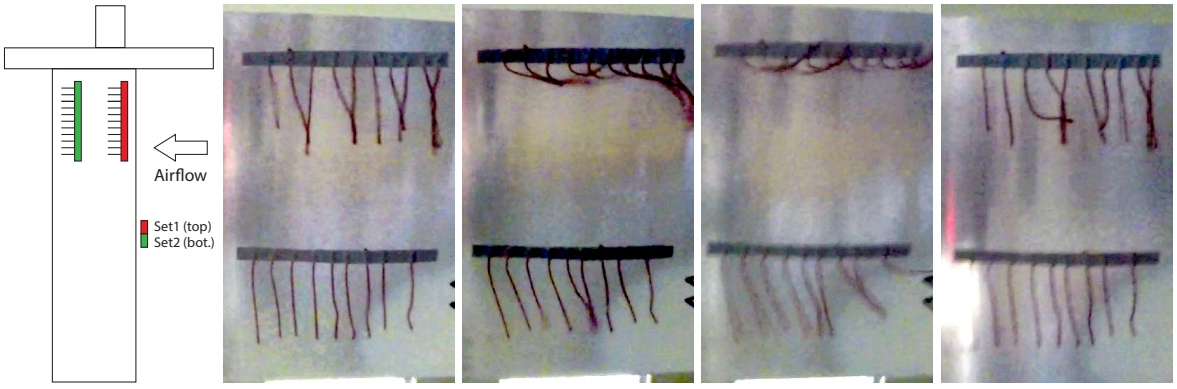

(a) Position of the tufts on the NLPF (b) t_1: beginning of the half cycle, small increasing pitch angle and attached flow (c) t_2: middle of the half cycle, large pitch angle & separation of the airflow on the leading edge (d) t_3: middle of the half cycle, large pitch angle & separation of the airflow on both the leading and trailing edges (e) t_4: end of the half cycle, small decreasing pitch angle and attached flow

Figure 8: Pictures of wool tufts on the wing during a cycle of half period of stall flutter at 14.9 m/s. The air flows from the top to the bottom on pictures (b) to (e).

to the green one, lies near the trailing edge. The following phenomena occur:

- t_1: the pitch angle is small and increasing, the tufts stick to the wing because the airflow is attached.
- t_2: the pitch angle is large and the front line of tufts (top) is detached from the wing which indicates separation of the airflow near the leading edge. The second line of tufts is much less affected by separation than the first line.
- t_3: the pitch angle is larger than at t_2. The airflow is now separated on both the leading and trailing edges.
- t_4: the pitch angle is small and the airflow is re-attached on the wing.

Figs.9 depicts the variation of $\ddot{\Phi}$ RMS acceleration (a) Φ RMS displacement (b) with airspeed. There are significant qualitative differences between Fig.7 and Fig.9. The acceleration increases very slowly between 11.5 and 13.5 m/s. Then its amplitude is

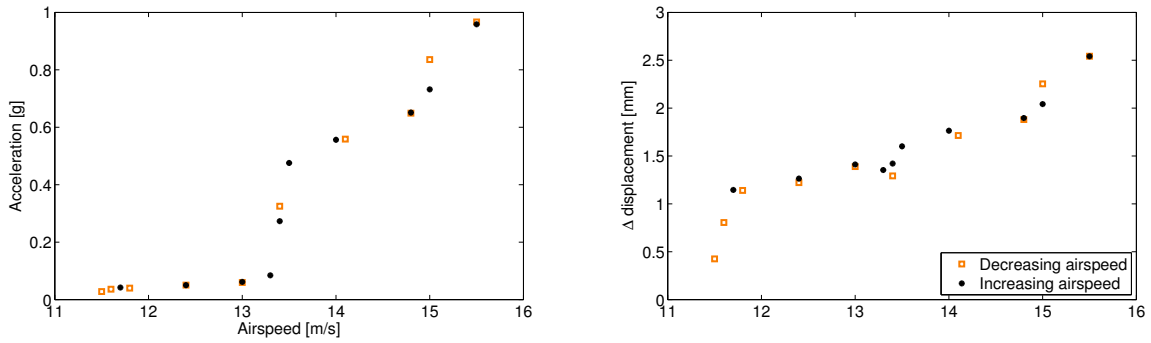

(a) RMS acceleration (b) RMS displacement

Figure 9: Bifurcation diagram of ϕ the plate deformations DOF

increased by a factor of 10 after the jump. It increases slowly again after the jump until a second jump occurs at 15m/s, albeit much smaller than the first one. The displacement diagram shows a smooth increase in RMS displacements with airspeed without any jump. High amplitude acceleration and low amplitude displacement suggests vibrations of the flat plate.

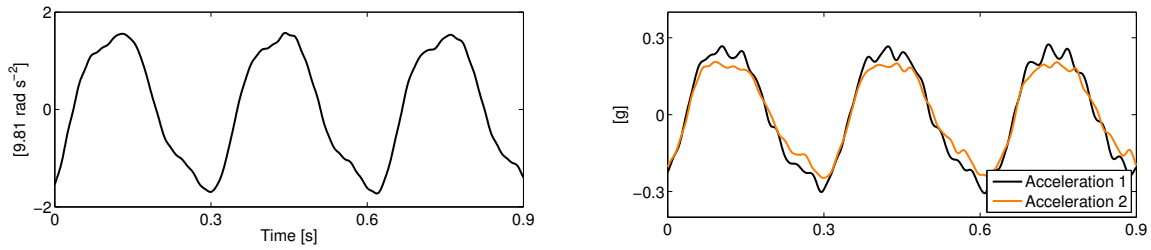

(a) Pitch acceleration (b) A_1 & A_2 accelerations

Figure 10: Time series of the LCO response at 13 m/s

Figs.10 and 11 plot the comparison of the time series of the pitch accelerations $\ddot{\theta}$ and the measurements of the accelerometers A_1 & A_2 respectively before and after the jump. Below the jump speed, a single important harmonic at the LCO fundamental frequency f_0 around 3 Hz dominates the dynamics and very small components at higher frequency can be noticed. Above the jump speed the pitch acceleration's frequency reaches 4 Hz and the $4f_0$ harmonic becomes large but the motion is still dominated by the fundamental frequency. The accelerations A_1 & A_2 on the other hand see their higher frequency components become as large as the 4Hz component and they are not in phase anymore. This also suggests vibrations of the flat plate.

3.2.3 LIMIT CYCLE OSCILLATION FREQUENCY VARIATION WITH AIRSPEED

Waterfall plots are depicted in Fig.12. They plot the FFT of the LCO responses at different airspeed and demonstrate the frequency values of all the peaks. It looks smooth but the vertical axis is not continuous. Fig.12(left) concerns the pitch frequencies and features the following peaks:

- The fundamental frequency, f_0, lies at 2.9Hz at 11.5 m/s and reaches 4.1 Hz at 15.5 m/s.
- A small third harmonic, $3f_0$, lies at 11.5m/s and its strength does not grow with airspeed compared to the f_0.

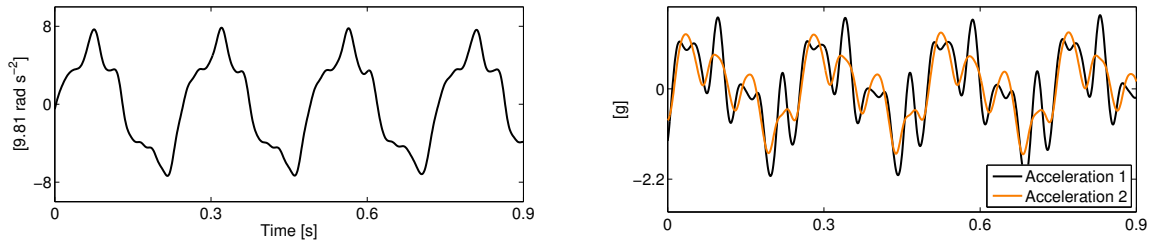

(a) Pitch acceleration

(b) A_1 & A_2 accelerations

Figure 11: Time series of the LCO response at 13.5 m/s

- The fourth and sixth harmonics, $4f_0$ and $6f_0$ emerge after the jump (13.5 m/s) and their strength does not grow with airspeed compared to f_0 either.
- The fifth harmonic, $5f_0$ appears after the jump and its amplitude increases slightly with airspeed compared to the amplitude of the fundamental frequency.

Fig.12(right) displays the evolution of the frequency of the accelerometers A_1 & A_2. It features the following peaks:

- The fundamental frequency, f_0 lies at 2.9 Hz at 11.5 m/s and reaches 4.1 Hz at 15.5 m/s.
- The second harmonic, $2f_0$ contributes to the motion from 11.5m/s but its strength explodes after the jump.
- The fourth and sixth harmonics, $4f_0$ and $6f_0$ start at small amplitude right before the jump (13.4 m/s) and their strength becomes similar to the strength of the fundamental harmonic after the jump (13.5 m/s). It is interesting to notice that the fourth harmonic is strong on both A_1 and A_2 while the sixth one is only affecting A_1 which suggests that they have different mode shapes.
- The third and fifth harmonics and a few other small peaks emerge as airspeed increases but their strength is very small and they to not contribute greatly to the dynamics of the system.

The origin of these spatial differences of accelerations can be investigated by plotting mode-shapes of the wind-on system. These modes-shapes are measured using 5 accelerometers placed on the trailing edge of the flat plate as displayed in Fig.13(a). This accelerometers setup does not allow the quantification of torsional effects but the first torsion mode is at much higher frequency and energy than the modes considered here. Moreover torsion would lead to a linear increase of the acceleration as we move towards the tip of the wing and it would be noticed on the mode shapes. The mode shapes of the strongest modes are the following:

- Fig.13(b) depicts the fundamental LCO mode at 4.1 Hz. All the accelerometers measure a large acceleration in phase, which suggests a motion dominated by the second mode. The measurements also suggest the presence a small modal component similar to the first mode.
- Fig.13(c) displays the mode shape of the second harmonic. It is similar to the third wind-off mode and their frequencies are rather close (8.2 Hz - 9.6 Hz). This means that there might be modal interactions.
- Fig.13(d) shows the mode shape of the fourth harmonic, which does not look like any other wind-off mode shape. Its frequency is not close to any other wind-off modal frequency either.
- Fig.13(e) plots the mode shape of the sixth harmonic. It is similar to the fourth wind-off mode and their frequencies are close as well: 25 Hz - 27.3 Hz, which means that there also might be modal interactions. Wind-on shaker tests are planned in the near future to evaluate the variation of frequency of the flexible modes with the airspeed and with the amplitude of the excitation to determine whether there is modal interaction.

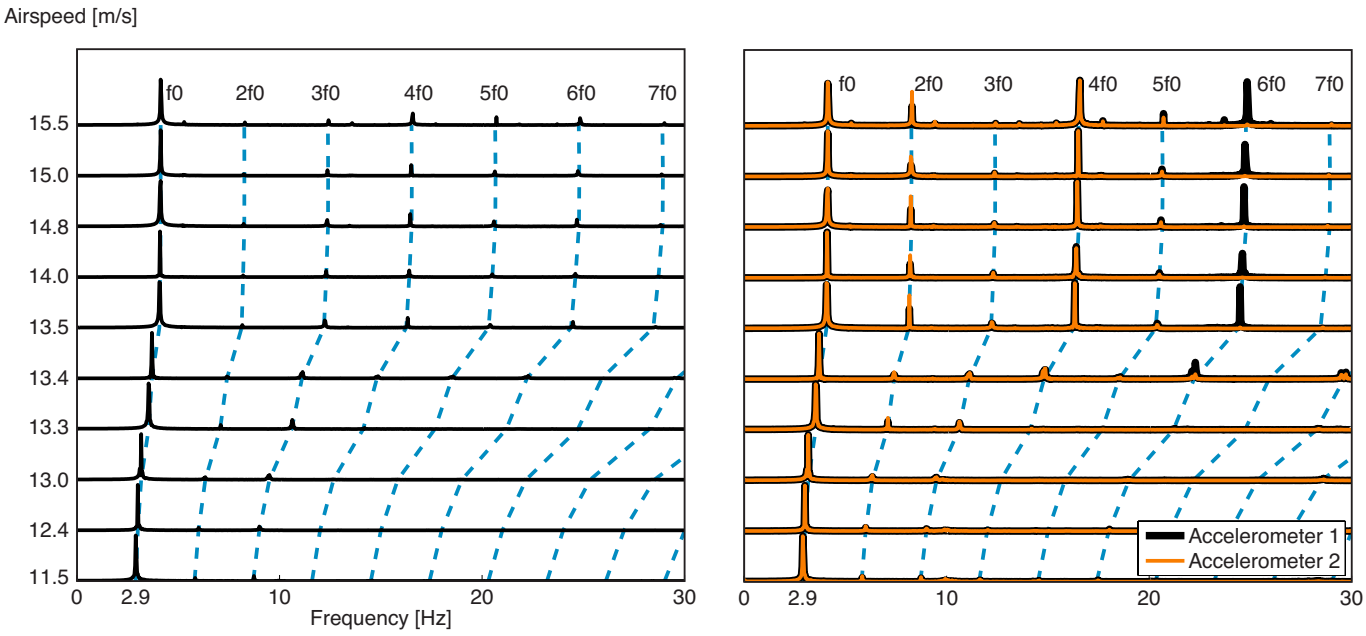

Figure 12: Waterfall plot of the pitch acceleration $\ddot{\theta}$ (left) and of the accelerations A_1 & A_2 (right)

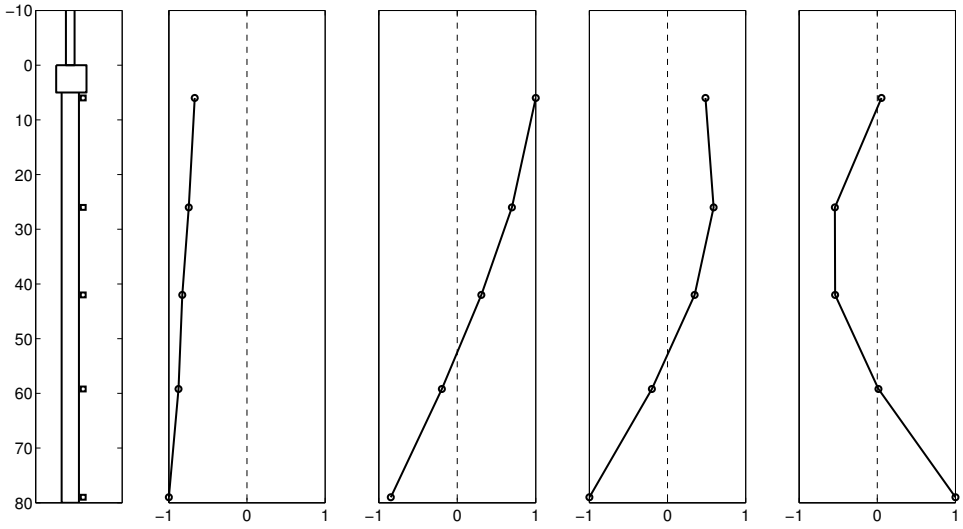

(a) Position of the accelerometers (b) Fundamental frequency: $f_0 = 4.1Hz$ (c) Second harmonic: $2f_0 = 8.2Hz$ (d) Fourth harmonic: $4f_0 = 16.4Hz$ (e) Sixth harmonic: $6f_0 = 24.6Hz$

Figure 13: Mode shapes of the strongest harmonics of the NLPFW at 14.9 m/s

4 DISCUSSION OF THE RESULTS

All the results presented above highlight the presence of an initial supercritical Hopf bifurcation at 11.5 m/s and two hypotheses were made to explain the jump at 13.5 m/s:

1. The jump is due to internal resonance. In this case the bifurcation diagram looks like Fig.14(a): the initial branch is due to the hardening nonlinearity and the jump is due to internal resonance between the nonlinear stiffness and higher modes. The separation of the airflow highlighted using wool tufts is just a result of the large amplitude of the pitch oscillations.
2. The jump is the consequence of stall flutter. Such a bifurcation diagram is drawn in Fig.14(b): the initial branch is still due to the hardening nonlinearity but it intersects with a subcritical stall flutter branch at the jump velocity. The separation of the airflow, shown using wool tufts, is the origin of the jump and the emergence of high frequency plate harmonics is just a consequence of the large amplitude of the motion.

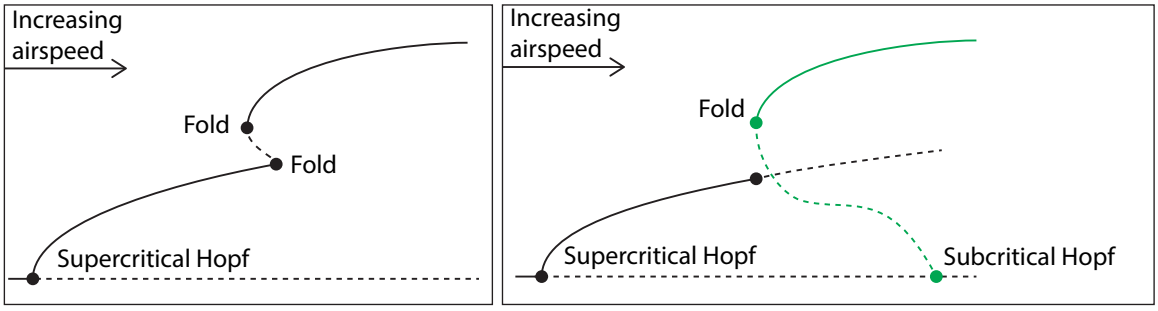

(a) Amplitude jump due to modal interactions

(b) Amplitude jump due to stall flutter

Figure 14: Theoretical bifurcations of the NLPFW

5 CONCLUSION

This study presents a new aeroelastic apparatus characterised by a low structural damping, continuous hardening and no hysteresis thanks to a bearing-free design. Unlike most setups studied in the past the flutter is caused by pitch and flap instead of pitch and plunge. It exhibits classical flutter characteristics for airspeeds between 0 and 11.5 m/s. Then the amplitude is limited by the structural hardening which leads to limit cycle oscillations. At 13.5 m/s a jump occurs that leads to strong pitching oscillations and vibrations of the flat plate. It is still not clear if this jump in amplitude is a result of internal resonance i.e. they are the cause of the jump or if they are just a consequence of the increase in the pitching amplitude. Further testing is planned with shakers or inertial exciters to help understand the non-linear dynamics of the structural system and to study the evolution of the third and fourth wind-off modes with the airspeed.

6 ACKNOWLEDGMENTS

The authors would like to acknowledge the financial support of the European Union (ERC Starting Grant NoVib 307265).

7 REFERENCES

[1] **Amandolese X. Michelin S. Choquel M.**, Low speed flutter and limit cycle oscillations of a two-degree-of-freedom flat plate in a wind tunnel, Journal of Fluids and Structures, Vol. 43, pp. 243-255, 2013

[2] **Abdul Razak N. Andrianne T. Dimitriadis G.**, Flutter and Stall Flutter of a Rectangular Wing in a Wind Tunnel, AIAA Journal, Vol. 49, No. 10, 2011

[3] **Abduk Razak N. Rothkegel J.I. Dimitriadis G.**, Experiments on a pitch-plunge wing undergoing limit cycle oscillation, Proceedings of the Structural Dynamics and Materials Conference, Honolulu, 2012

[4] **Dimitriadis G. Li J.**, Bifurcation Behavior of Airfoil Undergoing Stall Flutter Oscillations in Low-Speed Wind Tunnel, AIAA Journal, Vol. 47, No. 11, pp. 2577-2596, 2009

[5] **Poirel D. Mendes F.**, Experimental Investigation of Small Amplitude Self-Sustained Pitch-Heave Oscillations of a NACA0012 Airfoil at Transitional Reynolds Numbers, AIAA Journal, Vol. 52, No. 8, pp. 1581-1590, 2014

[6] **Mukhopadhvay V.**, Transonic Flutter Suppression Control Law Design Using Classical and Optimal Techniques with Wind-Tunnel Results, Proceedings of Structural Dynamics and Materials conference, St. Louis, 1999

[7] **O'Neil T. Gilliatt H. Strganac T.W.**, Invertigations of aeroelastic response for a system with continuous structural nonlinearities, Proceedings of the Structural Dynamics and Materials Conference, Salt Lake City, 1996

[8] **Silva W.A. Strganac T.W. HAjj M.R.**, Higher-Order Spectral Analysis of a Nonlinear Pitch and Plunge Apparatus, AIAA Journal,

[9] **Dowell E.H. Clack R. Cox D. Curtiss Jr. H.C. Edwards J.W. Hall K.C. Peters D.A. Scanlan R. Simiu E. Sisto F. Strganac T.W.**, A Modern Course in Aeroelasticity, Kluwer Academic Publishers, 2004

[10] **Abdelkefi A. Vasconcellos R. Nayfeh A.H. Hajj M.R.**, An Analytical and experimental investigation into limit-cycle oscillations of an aeroelastic system, Volume 71, Issue 1-2, pp. 159-173, 2012

[11] **Conner M.D Tang D.M. Dowell E.H. Virgin L.N.**, Nonlinear Behavior of a Typical Airfoil Section with Control Surface Freeplay: a Numerical and Experimental Study, Journal of Fluids an Structures, Vol. 11, pp. 89-109, 1997

[12] **Tang D.M. Dowell E.H.**, Aeroelastic Response Induced by Free Play, Part 2: Theoretical/Experimental Correlation Analysis, AIAA Journal, Vol. 49, No. 11, 2011

[13] **Hancock G.J. Wright J.R. Simpson A.**, On the teaching of the principles of wing flexure-torsion flutter, Aeronautical Journal, Vol. 89, pp. 285-305, 1985

[14] **Wright J.R. Cooper J.E.**, Introduction to Aircraft Aeroelasticity and Loads, John Wiley & Sons, 2007

[15] **Platten M.F. Wright J.R. Cooper J.E. Dimitriadis G.**, Idenfitication of a Nonlinear Wing Structure Using an Extender Modal Model, Journal of Aircraft, Vol.46, No.5, 2009